Nuclear Inst. and Methods in Physics Research B 435 (2018) 8–11

Contents lists available at ScienceDirect

Nuclear Inst. and Methods in Physics Research B

journal homepage: www.elsevier.com/locate/nimb

Radiation defect dynamics in 3*C*-, 4*H*-, and 6*H*-SiC studied by pulsed ion beams

L.B. Bayu Aji[a], J.B. Wallace[a,b], S.O. Kucheyev[a,*]

[a] Lawrence Livermore National Laboratory, Livermore, CA 94550, United States
[b] Department of Nuclear Engineering, Texas A&M University, College Station, TX 77843, United States

ABSTRACT

Radiation damage behavior of SiC depends on its lattice structure. Here, we use a pulsed-ion-beam method to study defect interaction dynamics in 6*H*-SiC and damage buildup in 4*H*- and 6*H*-SiC irradiated at 100 °C with 500 keV Ar ions. These results are compared with previously reported data for Ar-ion-irradiated 3*C*- and 4*H*-SiC. We find that, for these irradiation conditions, damage buildup in 3*C*- and 6*H*-SiC is statistically indistinguishable and is significantly more efficient than in 4*H*-SiC. Within a stimulated amorphization model, 4*H*-SiC is described by a reduced amorphization cross-section constant, while the point defect cluster production cross-section is the same (within experimental errors) for the three polytypes studied. Moreover, 4*H*-SiC exhibits slower defect relaxation dynamics than 3*C*- and 6*H*-SiC. These results clearly demonstrate the importance of the lattice structure in damage buildup and defect interaction dynamics in SiC.

1. Introduction

Silicon carbide is a prototypical nuclear ceramic material [1]. It is also a wide-band-gap semiconductor used in electronics, where ion implantation is a critical device processing step [2]. Understanding radiation damage in SiC is beneficial for both nuclear and electronic applications of this material. Hence, numerous previous studies of radiation effects in different polytypes of SiC have been reported (see, for example, [1–13]). Above room temperature, the accumulation of stable lattice disorder in SiC is dominated by so called dynamic annealing (DA) [3–13], which refers to the migration and interaction of point defects ballistically generated by the ion beam. These mobile (and, hence, unstable) point defects could interact with each other and with pre-existing otherwise stable defect structures in the lattice. The DA is typically experimentally manifested as the dependence of the defect formation efficiency on sample temperature, the defect generation rate, and the density of collision cascades. For regimes with pronounced DA, damage buildup in SiC is complex and remains poorly understood [1–13].

Defect migration and interaction processes depend on the lattice structure. Hence, in regimes with pronounced DA, damage buildup is expected to be different in different polytypes of SiC [11,9]. A recent pulsed ion beam study have indeed revealed a pronounced difference in defect interaction dynamics in 4*H*- and 3*C*-SiC bombarded at 100 °C with 500 keV Ar ions [11]. In the present paper, we study damage buildup and defect interaction dynamics in 6*H*-SiC and damage buildup in 4*H*-SiC bombarded at 100 °C with 500 keV Ar ions. We compare our findings with previous results for 3*C*- and 4*H*-SiC polytypes irradiated under the same conditions [9–12]. We find that, for these irradiation conditions, 3*C*- and 6*H*-SiC exhibit very similar damage buildup and defect interaction dynamics, while 4*H*-SiC behaves differently.

2. Experimental

We used single crystals of high-purity semi-insulating (0001) 4*H*-SiC and (0001) 6*H*-SiC obtained from II-VI, Inc. The crystal quality of as-received wafers was verified by measuring a minimum 2 MeV He ion channeling yield of ~ 1.5%, consistent across the wafer. To improve thermal contact, samples were attached to a Cu target holder with conductive silver paste.

The 4 MV ion accelerator (National Electrostatics Corporation, model 4UH) at Lawrence Livermore National Laboratory was used for both ion irradiation and ion beam analysis. Samples were bombarded at 100 °C with 500 keV ^{40}Ar ions at 7° off the sample normal direction to minimize channeling. All irradiation experiments were performed in a broad beam mode (rather than in a raster mode) [14]. In each irradiation run with pulsed beams, the total ion fluence (Φ) was split into a train of equal square pulses. Each pulse had the same dose rate (F_{on}) of 1.9×10^{13} cm^{-2} s^{-1} and a duration (t_{on}) of 1 ms and was separated from the subsequent pulse by t_{off} that was varied between 0 and 100 ms.

* Corresponding author.
E-mail address: kucheyev@llnl.gov (S.O. Kucheyev).

https://doi.org/10.1016/j.nimb.2018.03.026
Received 21 August 2017; Accepted 16 March 2018
Available online 28 March 2018
0168-583X/

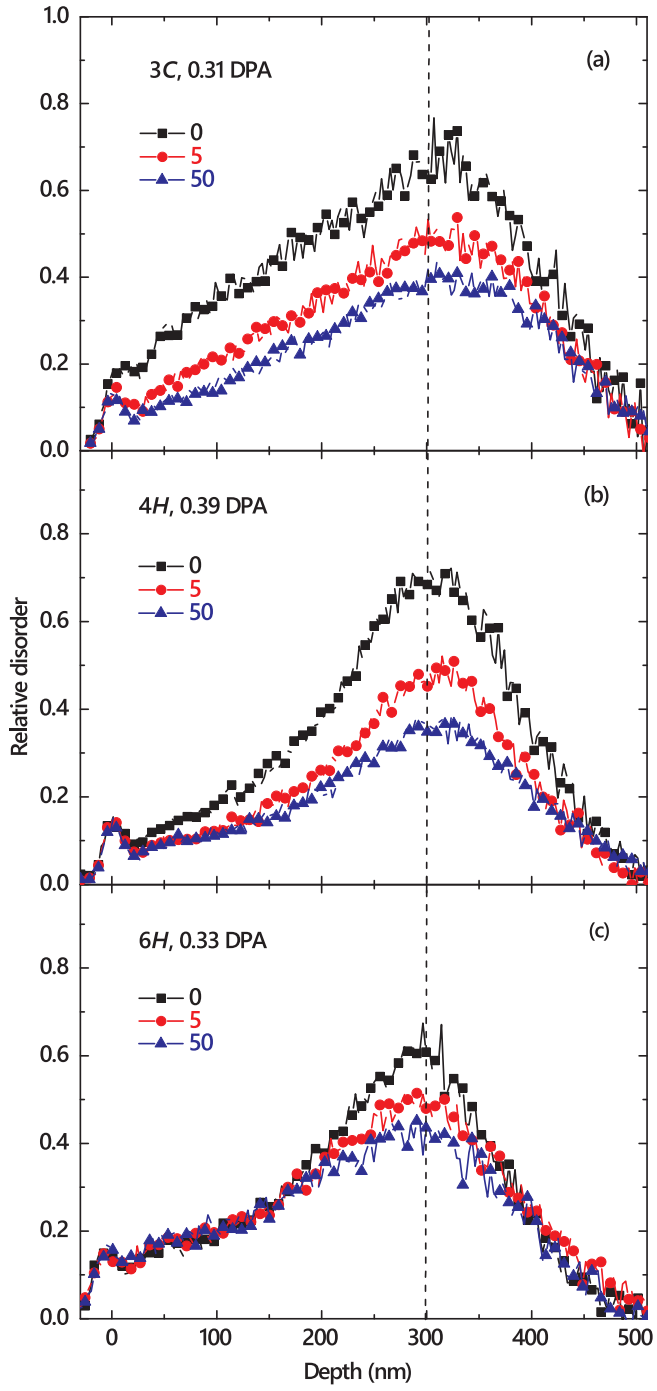

Fig. 1. Selected depth profiles of relative disorder in (a) 3*C*-, (b) 4*H*-, and (c) 6*H*-SiC irradiated at 100 °C with a pulsed beam of 500 keV Ar ions with $F_{on} = 1.9 \times 10^{13}$ cm^{-2} s^{-1}, $t_{on} = 1$ ms, and different t_{off} values given in the legends (in units of ms). The total fluences used are also shown in the legends. For clarity, only every 10th experimental point is depicted. The vertical dashed line shows the position of the maximum of the nuclear energy loss profile of Ar ions.

Depth profiles of stable lattice disorder in the Si sublattice were measured by ion channeling *ex-situ* at room temperature with 2 MeV $^4He^+$ ions incident along the [0001] direction and backscattered into a detector at 164° relative to the incident beam direction. Raw channeling spectra were analyzed with one of the conventional algorithms [15] for extracting depth profiles of relative disorder. Values of average relative bulk disorder (n, with $n = 1$ corresponding to full amorphization) were obtained by averaging depth profiles of relative disorder over 15 channels (~ 40 nm) centered on the bulk damage peak

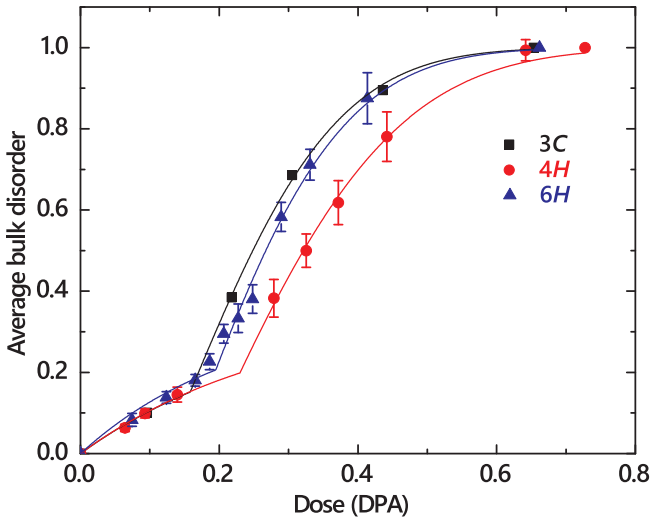

Fig. 2. Fluence dependencies of average relative bulk disorder in 3*C*-, 4*H*-, and 6*H*-SiC bombarded at 100 °C with a continuous beam of 500 keV Ar ions with a dose rate of 1.9×10^{13} cm^{-2} s^{-1}. Solid lines are results of fitting with a stimulated amorphization model described in the text.

maximum. Error bars of n are standard deviations.

The depth profile of the lattice vacancies ballistically-generated by 500 keV Ar ions was calculated with the TRIM code (version SRIM-2013.00, full cascade calculations) [16] as described in [13] with an atomic concentration of SiC of 9.64×10^{22} cm^{-3} and threshold energies for atomic displacements of 20 and 35 eV for C and Si sublattices, respectively. To convert to displacements per atom (DPA) at the maximum of the nuclear energy loss profile, ion fluence (in units of ion cm^{-2}) is multiplied by 8.5×10^{-16} DPA cm^2 ion^{-1}.

3. Results and discussion

3.1. Damage buildup for continuous beam irradiation

Figs. 1(a)–1(c) compare damage–depth profiles for the three polytypes irradiated at 100 °C to similar total fluences with continuous (i.e., $t_{off} = 0$) and pulsed beams with different t_{off} values (given in the legends) and all the other irradiation parameters kept the same. In this and the following two figures, the new results for damage buildup (with a continuous ion beam) in 4*H*-SiC and 6*H*-SiC and new defect dynamics results (with a pulsed ion beam) for 6*H*-SiC are compared with previous data for 3*C*-SiC and 4*H*-SiC taken from [10,11], respectively. It is seen from Fig. 1 that, for all three polytypes, depth profiles are bimodal, with the main broad peak centered on the maximum of the nuclear energy loss profile (marked by a vertical dashed line) and the second much smaller intensity peak at the sample surface. Hence, the sample surface in all three polytypes appears to have a limited role in damage accumulation for these irradiation conditions.

Fig. 2 shows bulk damage buildup curves [i.e., $n(\Phi)$ dependencies for continuous beam bombardment] for the three polytypes studied. It is seen from Fig. 2 that, within experimental errors, damage buildup curves for 3*C*- and 6*H*-SiC overlap, while 4*H*-SiC exhibits a lower damage buildup efficiency for fluences $\gtrsim 0.2$ DPA. All three damage buildup curves have a sigmoidal shape, which is consistent with a number previous reports [3,8,9,12,13]. Such a sigmoidal shape of $n(\Phi)$ dependencies suggests nucleation-limited (i.e., stimulated) defect accumulation. Shown in Fig. 2 by solid lines are results of fitting with a phenomenological stimulated amorphization model from [9]. Within this model, the total damage level is given by the following expressions:

Table 1
Effective time constant of DA (τ), the DA efficiency (ξ_{DA}), and parameters of the stimulated amorphization model, described in the text, for three different polytypes of SiC bombarded at 100 °C with 500 keV Ar ions.

Polytype	τ (ms)	ξ_{DA} (%)	$\sigma_{cluster}$ (DPA^{-1})	ξ_{amorph} (DPA^{-2})	Φ_{crit} (DPA)	Φ_{amorph} (DPA)
3*C*	3.4 ± 0.3	44.4 ± 0.8	3.5 ± 0.5	25.1 ± 1.3	0.16 ± 0.01	0.51 ± 0.01
4*H*	4.8 ± 0.5	53.3 ± 1.3	3.5 ± 0.4	16.5 ± 1.1	0.23 ± 0.01	0.65 ± 0.02
6*H*	3.1 ± 0.4	33.3 ± 1.1	4.4 ± 0.5	24.6 ± 1.8	0.19 ± 0.01	0.53 ± 0.02

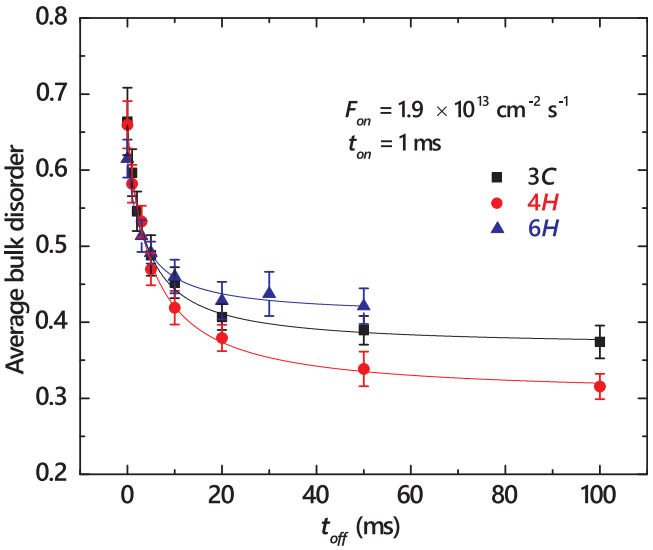

Fig. 3. Average relative bulk disorder in 3*C*-, 4*H*-, and 6*H*-SiC bombarded at 100 °C with a pulsed beam of 500 keV Ar ions with $F_{on} = 1.9 \times 10^{13}$ cm^{-2} s^{-1} and $t_{on} = 1$ ms as a function of the passive portion of the beam duty cycle (t_{off}). Fitting curves with the second order decay equation are shown by solid lines.

$$f_{total} = f_{amorph} + f_{cluster} = f_{amorph} + f_{cluster}^{sat}[1-\exp(-\sigma_{cluster}\Phi)](1-f_{amorph}),$$
$$f_{amorph} = h(\Phi-\Phi_{crit})(1-\exp[-\tfrac{\xi_{amorph}}{2}(\Phi^2-\Phi_{crit}^2)]). \quad (1)$$

Here, f_{amorph} is the fraction of atoms in the amorphous phase, $f_{cluster}$ is the atomic fraction of stable point defect clusters, $\sigma_{cluster}$ is the cluster production cross-section, $f_{cluster}^{sat}$ is the maximum saturation fraction of defect clusters in the lattice, $h(x)$ is the Heaviside step function [$h(x) = 0$ for $x < 0$ and $h(x) = 1$ for $x \geq 0$], Φ_{crit} is the critical fluence above which amorphization proceeds, and ξ_{amorph} is the amorphization cross-section constant. We used $f_{cluster}^{sat} = 36\%$ and a fitting procedure described in detail in [13].

Fig. 2 shows that such a stimulated amorphization model provides an excellent fit for all the cases. Table 1 lists the fitting parameters: $\sigma_{cluster}$, ξ_{amorph}, and Φ_{crit} as well as the amorphization fluence (Φ_{amorph}, taken as the Φ corresponding to). It is seen from Table 1 that, within fitting errors, $\sigma_{cluster}$ is the same for all three polytypes, while ξ_{amorph} is much lower for 4*H*-SiC than for the other two polytypes. This quantifies the above statements that all three damage buildup curves in Fig. 2 essentially overlap for $\Phi \lesssim 0.2$ DPA and damage buildup becomes less efficient in 4*H*-SiC for higher fluences. A larger Φ_{crit} for 4*H*-SiC also reflects that the inflection point of the sigmoid is at higher fluence for 4*H*-SiC than for the other two polytypes. Interestingly, our recent systematic studies of 3*C*-SiC [9,12,13] have also revealed that ξ_{amorph}, rather than $\sigma_{cluster}$, is changing in damage buildup experiments with variable temperature, ion mass, and the dose rate. Hence, the amorphization process for $\Phi \gtrsim \Phi_{crit}$ is critically sensitive to the lattice structure, dose rate, collision cascade density, and sample temperature, while the accumulation of point defect clusters appears to be insensitive to these parameters.

3.2. Defect relaxation dynamics studied by the pulsed ion beam method

Fig. 1 also shows that, for all three polytypes irradiated with a pulsed Ar ion beam, n decreases with increasing t_{off}, while the damage level at the sample surface remains unchanged, suggesting different dynamic mechanisms of bulk and surface disordering. This behavior is qualitatively similar to that found in previous studies (with pulsed beams of 500 keV Ar ions) of 3*C*-SiC at 100 °C and 4*H*-SiC in the T range of 25–250 °C [10–12].

Fig. 3 summarizes $n(t_{off})$ dependencies for the three polytypes. Solid lines in Fig. 3 are fits of the data via the Marquardt–Levenberg algorithm [17] with the second order decay equation ($n(t_{off}) = n_\infty + \frac{n(0)-n_\infty}{1+\frac{t_{off}}{\tau}}$). Here, τ is the effective time constant of DA, and n_∞ is relative disorder for $t_{off} \gg \tau$. All the $n(t_{off})$ dependencies from Fig. 3 obey the second order decay better than the first order (i.e., exponential) decay. Table 1 lists the two fitting parameters: τ and ξ_{DA}, which is the DA efficiency defined as before [10–12]: $\xi_{DA} = \frac{n(0)-n_\infty}{n(0)}$. As discussed in detail previously [18], for our choice of pulsing parameters, ξ_{DA} is the magnitude of the dose-rate effect; i.e., the difference between n for continuous beam irradiation with dose rates of $F = F_{on}$ and $F \to 0$. Table 1 shows that the three polytypes are characterized by different ξ_{DA} values, with 4*H*-SiC having the largest ξ_{DA}. The DA time constant (τ) is also larger for 4*H*-SiC than for the other two polytypes. These findings can be used to test future theoretical studies of the energetics of the defects dominating DA processes in different polytypes of SiC.

4. Summary

In summary, we have presented a comparative study of damage buildup and defect interaction dynamics in the three main polytypes of SiC (3*C*,4*H*, and 6*H*) bombarded at 100 °C with 500 keV Ar ions. Our results have clearly demonstrated that DA in SiC depends on the lattice structure. These observations call for future systematic studies of both damage buildup and defect interaction dynamics at different temperatures and for irradiation conditions with different cascade densities. These experimental results can be used to benchmark models of radiation damage in different polytypes of SiC.

Acknowledgments

This work was funded by the Nuclear Energy Enabling Technology (NEET) Program of the U.S. DOE, Office of Nuclear Energy and performed under the auspices of the U.S. DOE by LLNL under Contract DE-AC52-07NA27344. J.B.W would like to acknowledge the LGSP for funding.

References

[1] L.L. Snead, T. Nozawa, Y. Katoh, T.S. Byun, S. Kondo, D.A. Petti, J. Nucl. Mater. 371 (2007) 329.
[2] A. Fissel, Phys. Rep. 379 (2003) 149.
[3] W.J. Weber, N. Yu, L.M. Wang, J. Nucl. Mater. 253 (1998) 53.
[4] A.Yu. Kuznetsov, J. Wong-Leung, A. Hallén, C. Jagadish, B.G. Svensson, J. Appl. Phys. 94 (2003) 7112.
[5] M. Posselt, L. Bischoff, J. Teichert, A. Ster, Appl. Phys. Lett. 93 (2003) 1004.
[6] Y. Zhang, W.J. Weber, W. Jiang, C.M. Wang, V. Shutthanandan, A. Hallén, J. Appl.

Phys. 95 (2004) 4012.
[7] E. Wendler, T. Bierschenk, W. Wesch, E. Friedland, J.B. Malherbe, Nucl. Instrum. Methods B 268 (2010) 2996.
[8] A. Debelle, L. Thome, D. Dompoint, A. Boulle, F. Garrido, J. Jagielski, D. Chaussende, J. Phys. D: Appl. Phys. 43 (2010) 455408.
[9] J.B. Wallace, L.B. Bayu Aji, T.T. Li, L. Shao, S.O. Kucheyev, J. Appl. Phys. 118 (2015) 105705.
[10] J.B. Wallace, L.B. Bayu Aji, L. Shao, S.O. Kucheyev, Appl. Phys. Lett. 106 (2015) 202102.
[11] L.B. Bayu Aji, J.B. Wallace, L. Shao, S.O. Kucheyev, Sci. Rep. 6 (2016) 30931.
[12] L.B. Bayu Aji, J.B. Wallace, S.O. Kucheyev, Sci. Rep. 7 (2017) 44703.
[13] L.B. Bayu Aji, T.T. Li, J.B. Wallace, S.O. Kucheyev, J. Appl. Phys. 121 (2017) 235106.
[14] M.T. Myers, S. Charnvanichborikarn, L. Shao, S.O. Kucheyev, Phys. Rev. Lett. 109 (2012) 095502.
[15] K. Schmid, Radiat. Eff. 17 (1973) 201.
[16] J.F. Ziegler, M.D. Ziegler, J.P. Biersack, Nucl. Instrum. Methods B 268 (2010) 1818.
[17] K. Levenberg, Q. Appl. Math. 2 (1944) 164.
[18] J.B. Wallace, L.B. Bayu Aji, L. Shao, S.O. Kucheyev, J. Appl. Phys. 118 (2015) 135709.